Science of the Total Environment 922 (2024) 171307

Contents lists available at ScienceDirect

Science of the Total Environment

journal homepage: www.elsevier.com/locate/scitotenv

Estimating the probability of occurrence of African dust outbreaks over regions of the western Mediterranean basin from thermodynamic atmospheric parameters

Pedro Salvador [a,*], Jorge Pey [b], Noemí Pérez [c], Andrés Alastuey [c], Xavier Querol [c], Begoña Artíñano [a]

[a] CIEMAT, Department of Environment - Joint Research Unit Atmospheric Pollution CIEMAT-CSIC, Av. Complutense 40, 28040 Madrid, Spain
[b] Instituto Pirenaico de Ecología (IPE), CSIC, Av. Montañana 1005, 50059 Zaragoza, Spain
[c] Institute of Environmental Assessment and Water Research (IDAEA), CSIC, c. Jordi Girona 18, 08034 Barcelona, Spain

HIGHLIGHTS

- African dust events degrade air quality in SW Europe.
- A new method for estimating the probability of dust events occurrence is proposed.
- Thermodynamic atmospheric variables were used as assessing parameters.
- Future estimations and past events can be assessed with this methodology.
- The methodology could be replicated elsewhere with adequate assessing parameters.

GRAPHICAL ABSTRACT

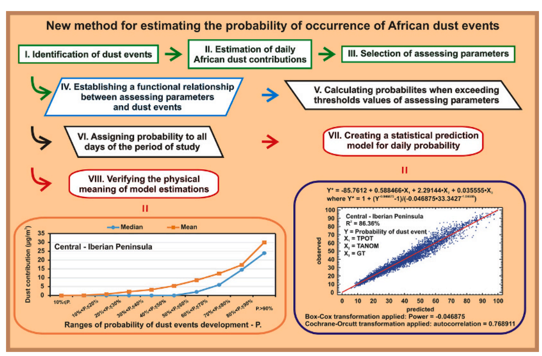

ARTICLE INFO

Editor: Pavlos Kassomenos

Keywords:
Air pollution
Desert dust
Atmospheric thermodynamics
Multilinear statistical models
Risk analysis
Trend analysis

ABSTRACT

Desert dust is currently recognized as a health risk factor. Therefore, the World Health Organization (WHO) is actively promoting the establishment of early warning systems for sand and dust storms. This study introduces a methodology to estimate the probability of African dust outbreaks occurring in eight different regions of the Iberian Peninsula and the Balearic Islands. In each region, a multilinear regression model was developed to calculate daily probabilities of dust events using three thermodynamic variables (geopotential thickness in the 1000–500 hPa layer, mean potential temperature between 925 and 700 hPa, and temperature anomalies at 850 hPa) as assessment parameters. All days with African dust transport over each study region were identified in the period 2001–2021 using a proven procedure. This information was then utilized to establish a functional relationship between the values of the thermodynamic parameters and the probability of African dust outbreaks occurring. The validation of this methodology involved comparing the daily probabilities of dust events generated by the models in 2001–2021 with the daily African dust contributions to PM_{10} regional background levels in each region. On average, daily dust contributions increased proportionally with the increase in daily probabilities, reaching zero for days with low probabilities. Furthermore, a well-defined seasonal evolution of

* Corresponding author.
E-mail address: pedro.salvador@ciemat.es (P. Salvador).

https://doi.org/10.1016/j.scitotenv.2024.171307
Received 18 December 2023; Received in revised form 19 February 2024; Accepted 25 February 2024
Available online 28 February 2024

probability values was observed in all regions, with the highest values in the summer months and the lowest in the winter period, ensuring the physical relevance of the models' results. Finally, upward trends were observed in all regions for the three thermodynamic parameters over 1940–2021. Thus, the probability of dust events development also increased in this period. It demonstrates that the aggravation of warm conditions in southern Europe in the last decades, have modified the frequency of North-African dust outbreaks over the western Mediterranean basin.

1. Introduction

Particulate matter (PM) emitted from arid and semi-arid surfaces, predominantly composed of mineral matter, is commonly referred to as desert dust. Annual emissions of desert dust into the troposphere range between 1.2 and 1.8 billion tonnes (Textor et al., 2006; Huneeus et al., 2011; Ginoux et al., 2012; Kok et al., 2017). Consequently, desert dust emerges as a significant contributor to the global aerosol burden (Textor et al., 2006).

The Sahara desert and the Sahel region in northern Africa are the most active global dust sources, emitting between 790 and 840 million tonnes annually. Other notable source regions include the Gobi and Taklamakan deserts in East Asia, the Sistan Basin and other regions of the Middle East, central Asia (Karakum desert), central Australia (Lake Eyre Basin), South America (Atacama and Patagonian deserts), South Africa, and the southern USA and northern Mexico (Prospero et al., 2002; Washington et al., 2003; Huneeus et al., 2011; Ginoux et al., 2010, 2012; Varga, 2012; Orlovsky et al., 2005; Alizadeh Choobari et al., 2013).

Key natural dust-emitting regions include topographic depressions with accumulated alluvium, dry lakes with unconsolidated fine-grained sediments, ephemeral streams-rivers, and inland basins known as playa-lakes (Prospero et al., 2002; Ginoux et al., 2012). Hooper and Marx (2018) estimated that globally dust emissions increased by a factor of 2.1 times after the Industrial Revolution. This change was associated with human activities such as the conversion of wildlands to agricultural landscapes and overgrazing, leading to the desiccation of lakes and ephemeral lakes worldwide, resulting in increased dust emissions (Gill, 1996; Stout, 2001; Orlove, 2005; Neff et al., 2008; Cook et al., 2009; Ma et al., 2010; Lee et al., 2012; Zucca et al., 2021, among others). The contribution of dust emissions from anthropogenic sources remains uncertain, with estimates ranging from 10 % to 50 % of the total (Tegen et al., 1996, 2004; Sokolik and Toon, 1996). This contribution is expected to rise in the future due to increasing human impact on land use and climate variability.

Dust source regions remain active throughout the year, with emission rates peaking in different periods depending on the region, such as spring and summer in northern Africa, summer and autumn in the Middle East, central Asia and Australia, autumn-winter in South America, summer in North and South America and southern Africa, and autumn in eastern Asia (Querol et al., 2019a).

The development of massive dust resuspension convective processes in source regions, coupled with the formation of nocturnal thermal inversions on their surface, results in the creation of dust layers at various altitudes, making them subject to long-range transport. Desert dust is then transported by prevailing synoptic air mass circulations and distributed across the planet. Major transport routes include movements from the Sahara and Sahel towards the Caribbean, South America, and Southern USA; from the Sahara to the Mediterranean basin; from the Gobi and Taklamakan deserts towards the Pacific Ocean; from southern USA towards Mexico and eastern USA; from South Africa towards the Atlantic Ocean; from South America to the southern Atlantic Ocean; from the Middle East towards central and southern Asia; from central Australia to different regions around; from Iceland towards Europe; and from Ukraine towards central Europe, among others (Griffin, 2007; Querol et al., 2019a and references therein).

Goudie and Middleton (2001) summarized some of the most significant environmental consequences of desert dust deposition on terrestrial and oceanic ecosystems. Dust additions play a crucial role in delivering nutrients and sediments to the oceans, especially in the North Atlantic Ocean. Additionally, they may enhance plankton productivity due to the iron content typically present in dust. On the flip side, dust can cause Caribbean-wide epidemics, diminishing coral reef vitality due to disease-spreading spores transported by African dust. A large amount of dust from the Sahara desert also reaches the Amazon Basin. It is loaded with phosphorus (an estimated 22,000 tons per year). This is an essential nutrient for plant proteins and growth, which the Amazon rain forest depends strongly on in order to flourish (Yu et al., 2015). Desert dust inputs to land surfaces also impact soil formation, and once in the atmosphere, they significantly influence the climate system (Alizadeh Choobari et al., 2014). Mineral dust directly affects the climate by scattering and absorbing solar and infrared radiation, semi-directly by altering atmospheric cloud cover through the evaporation of cloud droplets, and indirectly by acting as cloud and ice condensation nuclei, thereby altering the optical properties of clouds and potentially affecting precipitation formation (Miller and Tegen, 1998; Ackerman et al., 2000; Koren et al., 2004; Su et al., 2008, Rosenfeld and Woodley, 2000; Andreae et al., 2004).

Characterizing the environmental impact of desert dust can be highly complex, as illustrated by its influence on the Earth's radiative balance, which modifies certain atmospheric dynamics processes. This can have important implications on air quality near the surface. For instance, direct radiative forcing by desert dust plumes cools the air layers close to the surface while warming the air aloft them (Alizadeh Choobari et al., 2012). This alteration of the vertical temperature profile increases atmospheric stability within the lower troposphere. Consequently, a reduction in the mixing layer height has been detected in some Spanish cities during African dust outbreaks (ADO), compared to days without the influence of desert dust (Pandolfi et al., 2014; Salvador et al., 2019). The arrival of African dust layers not only increased the concentration of PM_{10} due to the contribution of desert dust but also elevated gaseous pollutants (NO_x and CO) and fine and ultrafine particles due to accumulated emissions from local anthropogenic sources in the reduced mixing layer.

In this context, the development of desert dust outbreaks significantly impacts air quality, particularly concerning coarse PM, over large receptor areas. Goudie (2014) reported maximum desert dust levels of 150–2500, 134–3006, 266–15,366, 312–5000, 123–65,112, and 700–5619 μg/m^3 of PM_{10} during dust events over southern Europe, eastern Asia, Australia, western Africa, North America, and the Middle East, respectively. African dust is currently assumed to be the largest PM_{10} source in regional background sites of the Mediterranean basin (Pey et al., 2013; Querol et al., 1998, 2004, 2009, 2019b; Rodríguez et al., 2001; among others). Dust transport towards western Mediterranean regions is caused by low-pressure systems over the Atlantic or North Africa, high pressures over the Mediterranean, or high pressures at upper levels over northwestern Africa, mainly in summer (Querol et al., 2009; Salvador et al., 2014, among others). ADO over the eastern Mediterranean generally originates in the spring-early summer and autumn periods due to thermal lows moving eastwards throughout the Mediterranean (Moulin et al., 1998; Kubilay et al., 2000) or the combination of low pressures over North Africa with high pressures over the Middle East (Kallos et al., 2006). Pey et al. (2013) estimated that ADO frequency was higher in the eastern (31 % days of the year on average) than the western (23 %) side of the basin for the period 2001–2011. The eastern region is also affected by dust storms originating in the Negev and Middle East deserts (Basart et al., 2009). For this reason, the mean African dust inputs to PM_{10}, were approximately two-fold higher in the eastern locations of the Mediterranean (5.0 μg/m^3) compared to the western side (2.6 μg/m^3) during the period 2001–2011 (Pey et al., 2013). Thus, the phenomenology of ADO varies considerably across the Mediterranean basin concerning synoptic meteorological mechanisms, transported dust quantity, and seasonal frequency throughout the year.

Numerous studies have highlighted that ADO triggers exceedances of the PM_{10} daily limit value for health protection (set at 50 μg/m^3 in EU Directive 2008/50/EC on ambient air quality and a cleaner atmosphere in Europe) at air quality monitoring stations in Southern European countries (Achilleos et al., 2014; Aleksandropoulou and Lazaridis, 2013; Barnaba et al., 2017, 2022; Escudero et al., 2007a; Pey et al., 2013; Querol et al., 1998, 2004, 2009, 2019b; Salvador et al., 2013; among others).

Moreover, other studies have reported increases in mortality and morbidity indices due to PM_{10} exposure during ADO in these countries (Pérez et al., 2008, 2012; Stafoggia and the MED-PARTICLES Study Group, 2016; Díaz et al., 2017, among others). Tobias et al. (2019a, b) conducted a systematic review on the health effects of desert dust and sand storms based on 93 worldwide studies. The results indicated an overall impact of desert dust on cardiovascular mortality and respiratory morbidity, although the evidence was inconsistent when considering PM sources in different geographical areas. Recognizing the significant health risk posed by sand and dust storms, the WHO Air Quality Guidelines have specifically addressed these phenomena in their latest update (*WHO Global Air Quality Guidelines. Particulate Matter (PM2.5 and PM10), Ozone, Nitrogen Dioxide, Sulfur Dioxide and Carbon Monoxide*, 2021).

The guidelines advocate for the establishment of early warning systems for sand and dust storms by relevant authorities. Such systems aim to (i) inform exposed and vulnerable populations about behavioral measures to minimize the risks of high dust exposure levels and (ii) implement special policy and regulatory measures at the local and regional levels to decrease anthropogenic air pollution emissions during dust episodes (*WHO Global Air Quality Guidelines. Particulate Matter (PM2.5 and PM10), Ozone, Nitrogen Dioxide, Sulfur Dioxide and Carbon Monoxide*, 2021). Over the last decades, several numerical models, such as NAAPS (U.S. Navy, Christensen, 1997), SKIRON (University of Athens, Kallos et al., 2006), or Monarch (Barcelona Dust Regional Center, Pérez et al., 2011), among others, have been developed for forecasting surface dust concentration. Although these models have significantly improved their performance, current uncertainties in reproducing actual dust surface concentrations in specific regions may still be substantial (Querol et al., 2019a). Therefore, confirming the actual arrival of dust at the surface or high altitude over a given region still requires the analysis of surface PM concentration data and/or measurements with remote sensing instruments such as LIDAR.

In this study, we have evaluated the connections between the dust transport process towards specific areas of the Iberian Peninsula (IP) and the Balearic Islands (BI) and the variability of certain thermodynamic parameters over them. Some authors already used thermodynamic parameters to detect heat waves over areas of Europe. Sánchez-Benítez et al. (2018) developed an algorithm to detect heatwaves events over regions of western and central Europe, using temperature anomalies at 850 hPa (TANOM) for the climatological period 1981–2010. Sousa et al. (2019) identified the development of summer heat waves produced by Saharan air masses in areas of the IP, when the 1000–500 hPa layer geopotential thickness (GT) and the mean 925–700 hPa layer potential temperature (TPOT) exceeded 580 decameters and 40 °C, respectively. Salvador et al. (2022) demonstrated that values of the thermodynamic variables GT, TPOT and TANOM were significantly higher over the IP–BI domain during the development of ADO compared to periods when such events did not occur. This study confirmed that ADO happened in all regions of this domain along all the year and under values of GT and TPOT lower than the threshold levels established by Sousa et al. (2019) to detect summer heat waves. However, no specific threshold values were defined for these variables whose exceedance was undoubtedly related to the occurrence of an ADO, or at least to a certain probability of occurrence of this phenomenon. Bearing this fact in mind, in this work we have evaluated the possibility that the exceedance of ranges of threshold values of GT, TPOT and TANOM over different regions of the IP-BI domain, were associated with a given probability of occurrence of ADO (PROB-ADO).

Bearing this fact in mind, in this work we have evaluated the possibility that the exceedance of ranges of threshold values of GT, TPOT and TANOM over different regions of the IP-BI domain, were associated with a given probability of occurrence of ADO (PROB-ADO). Moreover, this evaluation has allowed us to develop a methodology for generating multilinear models that provide estimations of PROB-ADO in each study area based on daily values of the three thermodynamic parameters. This approach aligns well with the WHO Air Quality Guidelines, specifically the recommendation to create early warning systems to alert the population and encourage personal measures to minimize the short-term health effects of sand and dust storms (*WHO Global Air Quality Guidelines. Particulate Matter (PM2.5 and PM10), Ozone, Nitrogen Dioxide, Sulfur Dioxide and Carbon Monoxide*, 2021).

The occurrence and development of ADO are influenced by atmospheric dynamic factors and desertification processes (Heffernan, 2016; Hooper and Marx, 2018). These processes are notably sensitive to changes in various climate components and forcings (IPCC, 2023). However, recent studies present conflicting findings regarding the impact of climate change on the frequency and intensity of ADO in regions spanning the Caribbean Sea and the Mediterranean and Euro-Atlantic sectors (Prospero and Lamb, 2003; Thomas and Nigam, 2018; Sousa et al., 2019; Adame et al., 2022; Salvador et al., 2022; Cuevas-Agulló et al., 2023).

With the aim of demonstrating the usefulness of this methodology in detecting and evaluating variations in the development of ADO over a long period of time, statistical methods were also applied to check the occurrence of time trends of the PROB-ADO estimates in the period 1940–2021, over all regions of study.

2. Material and methods

2.1. Procedure for estimating daily PROB-ADO

The methodology applied in this study involves several stages (Fig. 1), detailed below.

2.1.1. Stage I: identification of ADO

Initially, it is imperative to identify, over the longest feasible time frame, the dates on which ADO occurred across the 8 study areas in the IP-BI domain (SE, SW, E, central, NE, N, and NW areas of the IP and the BI, Fig. 2), leading to increased PM levels at the surface. This compilation of events enables the evaluation of the potential relationship between assessing parameters and ADO development.

For this work, a robust procedure based on the daily interpretation of various meteorological products was employed to identify all ADO episodes impacting PM_{10} levels in the 8 sub-domains from 2001 to 2021. This procedure is extensively described in Querol et al. (2013). Essentially, a combination of tools was utilized, all obtained or calculated from open-access repositories.

Firstly, daily air mass back-trajectories were computed with the HYSPLIT trajectory model (Stein et al., 2015). Five days backward air mass trajectories were run, ending at 12:00 UTC at three different arrival heights (750 m, 1500 m and 2500 m above ground level) over each region of study. They were interpreted together with synoptic meteorological maps to account for the transport of air masses from Northern Africa.

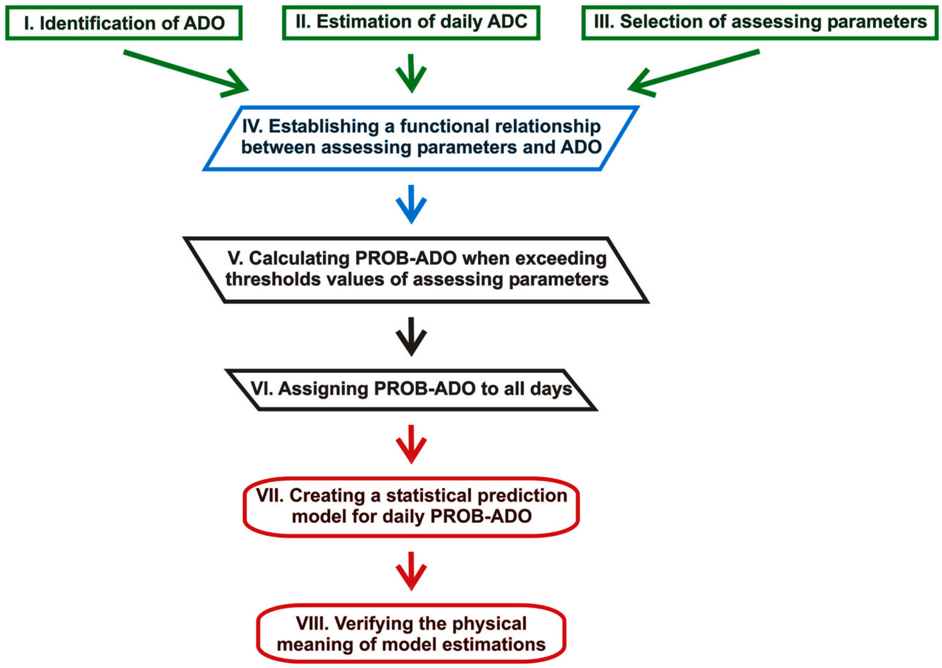

Fig. 1. Flow chart showing the stages of the methodology used. ADO: African dust outbreaks; ADC: African dust contribution; PROB-ADO: probability of occurrence of African dust outbreaks.

Subsequently, surface dust concentration maps generated by numerical models such as SKIRON - University of Athens (Kallos et al., 2006), DREAM/BSCDREAM8b and MONARCH - Barcelona Supercomputing Centre (Pérez et al., 2011) and NAAPs - Naval Research Laboratory (Christensen, 1997) and satellite imagery from MODIS – NASA (Justice et al., 2002) were analysed to detect the presence of dust plumes over the regions of study.

Finally, time series of PM_{10} levels from regional background monitoring sites (Barcarrota-SW, Viznar-SE, San Pablo-Central, Zarra-E, Bellver-BI, O Saviñao-NW, Valderejo-N, and Monagrega-NE, Fig. 2a) were acquired to assess the actual impact of ADO on PM_{10} concentrations (Querol et al., 2013).

2.1.2. Stage II: estimation of daily African dust contribution

Obtaining quantitative estimators of African dust contribution (ADC) in terms of PM concentration transported on ADO days is crucial to evaluate the intensity of ADO. Estimators of ADC can be derived from ad hoc procedures, such as those proposed by Escudero et al. (2007b) or Barnaba et al. (2022), or, when possible, from data on the crustal material content in PM samples obtained from chemical analysis (Alastuey et al., 2016).

In this study, datasets of daily mean PM_{10} levels from regional background monitoring sites were utilized to quantify the net ADC contribution for each ADO during the study period. The statistical procedure described in Escudero et al. (2007b) and Viana et al. (2010) was applied. It involves calculating the 30-day moving 40th percentile for regional background PM_{10} daily concentration time series. Previous studies have shown that this percentile adequately reproduces regional background levels over the IP-BI domain during periods with prevailing atmospheric advective conditions, i.e., without external PM contributions (Escudero et al., 2007b; Querol et al., 2013). Therefore, it facilitates the calculation of daily net ADC when subtracted from the daily mean PM_{10} regional background levels recorded in each study region during ADO development. This method is one of the official recommendations by the European Commission for evaluating ADO occurrence and quantifying ADC (Commission Staff Working Paper, 2011).

While PM_{10} measurements were available at a few regional background sites in Spain since 1995 (Querol et al., 1998), regular monitoring across all its regions did not commence until 2001. Additionally, many numerical models for predicting dust concentration were not fully developed before 2001. Consequently, the systematic identification of ADO in Spanish regions and the quantification of the associated ADC began in 2001. ADO catalogs, identified through the recognition procedure described in Section 2.1.1. and time series of ADC estimated using this statistical method have been widely utilized for scientific research purposes (Querol et al., 2009, 2019b; Pey et al., 2013; Salvador et al., 2013, 2014, 2019, 2022).

2.1.3. Stage III: selection of assessing parameters

Three thermodynamic parameters were chosen as assessing parameters:

1) GT: Geopotential thickness in the 1000–500 hPa layer measures the vertical distance in meters from the 1000 to the 500 hPa level. It indicates the warmth or coldness of this tropospheric layer. High values denote warm air, while low values signify cold air. GT increases due to warm air advection or diabatic warming (Galvin, 2016).
2) TPOT: This parameter represents the mean potential temperature between 925 and 700 hPa. The potential temperature of an air parcel is the temperature it would have if brought adiabatically to a standard pressure (usually 1000 mb). It is a conserved quantity for an air parcel in adiabatic motion, and under normal, stably stratified conditions, the potential temperature increases with height.
3) TANOM: This involves temperature anomalies at 850 hPa for the climatological period 1981–2010. A temperature anomaly is the difference from an average or baseline temperature, usually computed by averaging 30 or more years of temperature data. A positive anomaly indicates a temperature warmer than the baseline, while a negative anomaly indicates a cooler temperature.

High values of GT, TPOT, and TANOM denote warm, stable, low-density, and very dry air masses (Sousa et al., 2019) with the potential to be warmed by downward advection processes (Wallace and Hobbs, 2006).

As an illustrative example, Figs. 3a-f display maps of daily GT, TPOT,

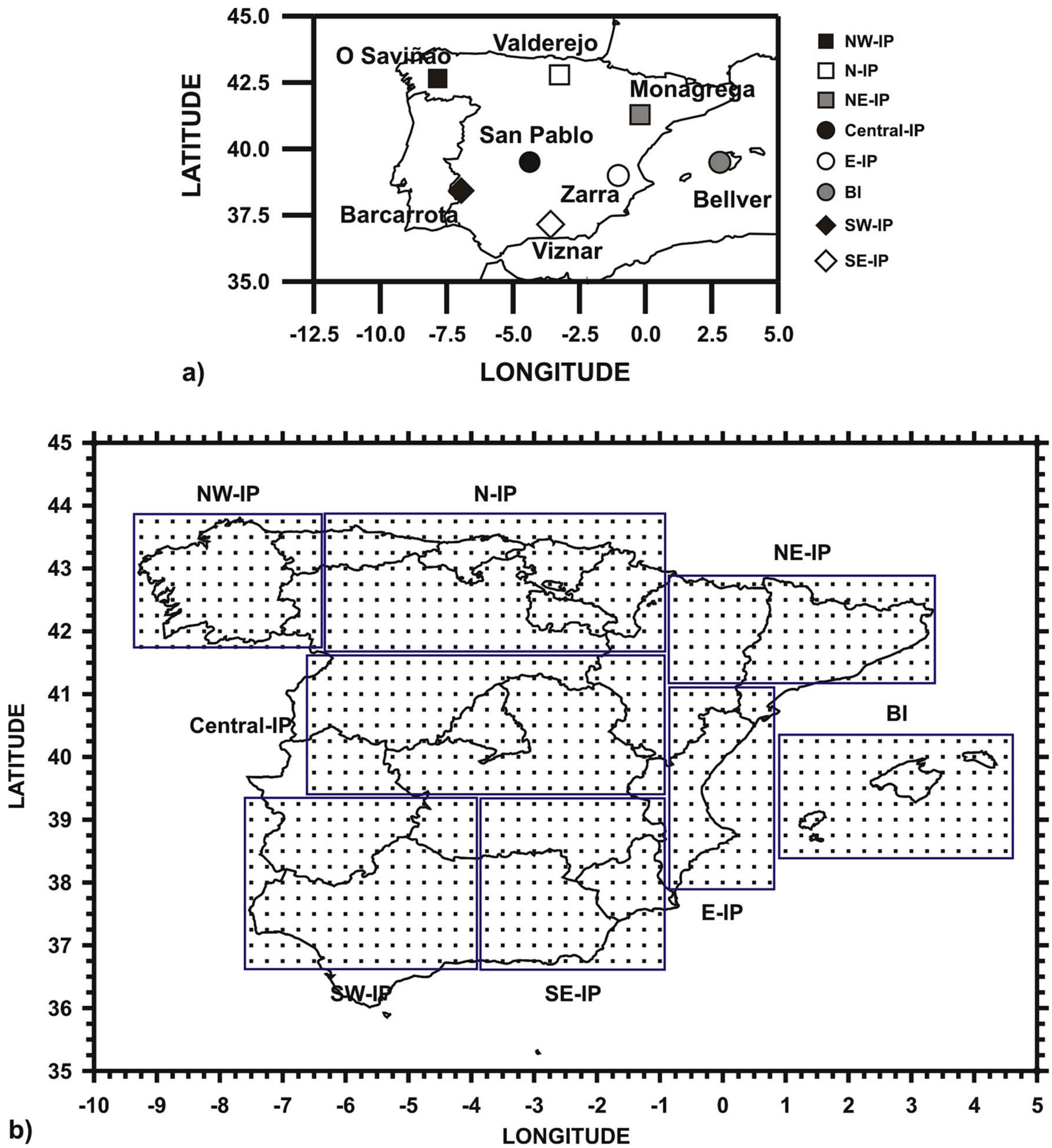

Fig. 2. Geographical location of the regional background air quality monitoring stations used for estimating the daily African dust contribution registered during African dust outbreaks (a) and of the grid points with data available in the meteorological fields for calculating thermodynamic parameters over the 8 sub-domains in the Iberian Peninsula (IP) and the Balearic Islands (BI) (b).

and TANOM values during two intense ADO affecting the IP-BI domain in different periods of the year. The first case (11-aug-2021) typifies a summer event with the advection of African air masses caused by a high-pressure system over northern Africa and the western Mediterranean basin (Fig. 3g). The African air masses entered the IP from the SE sector, traversed the BI, and moved over the IP in a diagonal path towards the north (Fig. 3j). Gradual increases in GT, TPOT, and TANOM values from SE-IP to NW-IP regions are evident in the maps (Figs. 3a-c). ADC levels decreased from the SE-IP, E-IP, and Central-IP regions (36–53 μg/m^3) to the SW-IP and NE-IP (33–34 μg/m^3), the BI (26 μg/m^3), and the N-IP regions (8 μg/m^3). The African dust plume did not reach the NW-IP region, where the lowest values of GT, TPOT, and TANOM were registered.

The second episode occurred in spring (31-mar-2021). During this period, the advection of African air masses towards the IP typically follows an Atlantic pathway, transporting dust from the Sahel region (Querol et al., 2004). This event resulted from the combined action of a low-pressure system to the SW of the IP and a high-pressure system extending over northern Africa, the Mediterranean basin, and central Europe (Fig. 3h). In this case, African air masses first affected regions in the western half of the IP (Fig. 3j), where GT, TPOT, and TANOM values were higher than in areas of the Eastern half and the BI (Figs. 3d-f). The highest value of ADC was recorded in the NW-IP region (108 μg/m^3), followed by the N-IP, Central-IP, SE-IP, and SW-IP regions (21–43 μg/m^3). In this instance, the BI was not affected by the dust episode. In all regions reached by dust during both events, the daily mean values of GT, TPOT, and TANOM far exceeded the mean values for August and March, respectively, in the period 2001–2021.

Finally, fields of hourly temperature and geopotential reanalysis data at several pressure levels were obtained from the "ERA5 hourly data on pressure levels from 1940 to present" dataset (Hersbach et al., 2023) to calculate GT, TPOT, and TANOM values. These data fields, downloaded

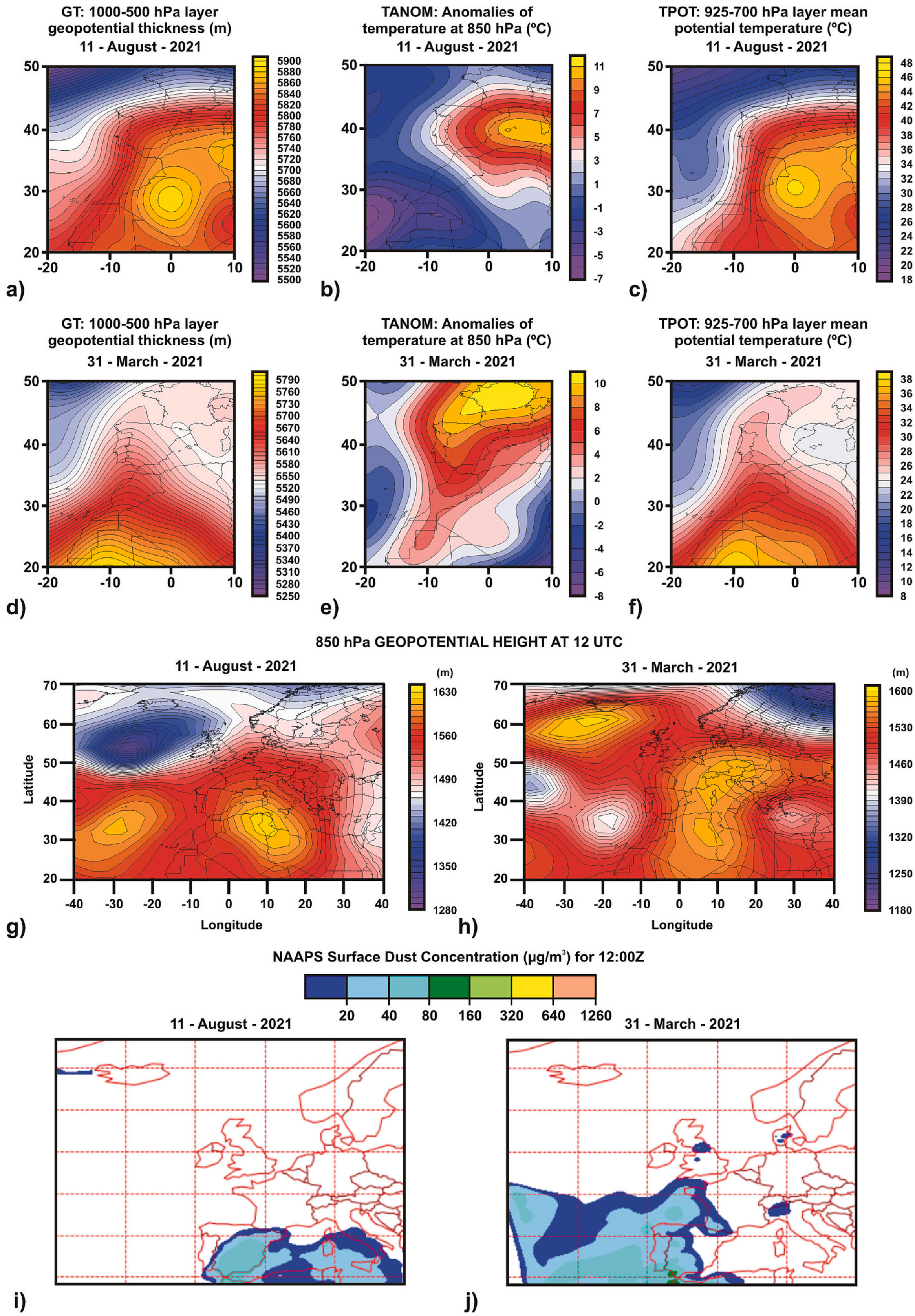

Fig. 3. Maps of daily mean values of thermodynamic parameters during the development of intense ADO over regions of the Iberian Peninsula and Balearic Islands on 11-August-2021 (a-c) and 31-March-2021 (d-f), of geopotential height in the 850 hPa level at 12 UTC (g-h) and of surface dust concentration over Europe provided by the NAAPS Global Aerosol Model (developed from Christensen, 1997) for both days (i-j).

from the Copernicus Climate Change Service (C3S) (2023) for the period 1940–2021, were distributed in each field in a 0.25° latitude x 0.25° longitude grid for each of the selected sub-domains of the IP-BI region (Fig. 2b). Subsequently, we calculated, for each day of the period 1940–2021 and for each region, the daily mean values of GT, TPOT, and TANOM.

2.1.4. Stage IV: establishing a functional relationship between assessing parameters and ADO

After selecting the assessing parameters, it is essential to analyze the functional relationship between their variability and the occurrence of ADO. In this study, the thermodynamic characteristics of the air masses in the study areas are explored to identify the arrival of African dust. Essentially, we aim to determine if the frequency of ADO in each area from 2001 to 2021 increased with rising values of GT, TPOT, and TANOM.

2.1.5. Stage V: calculating PROB-ADO when exceeding threshold values of assessing parameters

Building on the previous stages, the hypothesis that exceeding certain threshold values of assessing parameters correlates with specific PROB-ADO in each study area is evaluated. The list of ADO identified from 2001 to 2021 is utilized to calculate the number of occurrences in a region when GT, TPOT, and TANOM values surpass certain levels. The resulting PROB-ADO is computed as the ratio of positive cases (ADO episodic days with exceeded threshold values) to possible cases (all days with exceeded threshold values from 2001 to 2021). Percentiles of the time series of daily mean values of GT, TPOT, and TANOM are employed as threshold values. This study assumes the validity of these assessing parameters when there is a gradual increase in PROB-ADO as threshold values increase.

2.1.6. Stage VI: assigning PROB-ADO to all days

With threshold values for all possible PROB-ADO between 0 and 100 %, estimated PROB-ADO is assigned to each day of the study period based on associated daily mean values of GT, TPOT, and TANOM. For instance, if all three data points for a specific day exceed the 60 % probability threshold but not the 61 %, that day is assigned a PROB-ADO of 60 %.

2.1.7. Stage VII: creating a statistical prediction model for daily PROB-ADO

After estimating PROB-ADO for all days in all zones, the multiple linear regression procedure is employed to develop a statistical prediction model in each region. In this model, the independent variables are the assessment parameters (GT, TPOT, TANOM), and the dependent variable is PROB-ADO.

$$PROB - ADO = a1 \bullet TPOT + a2 \bullet TANOM + a3 \bullet GT + a4 \quad (1)$$

Once coefficients a1, a2, a3, and a4 are obtained, and the model's validity is confirmed through residual analysis, checking homoscedasticity, normality, and linear independence (Neter et al., 1990), PROB-ADO for a specific day can be estimated from the GT, TPOT, and TANOM data for that day using Eq. (1).

2.1.8. Stage VIII: verifying the physical meaning of model estimations

To validate PROB-ADO values predicted by the model from 2001 to 2021, the time series of daily ADC in each study area is used. If, as expected, many days with low to moderate PROB-ADO have no ADO occurrence (ADC is nil), the average ADC for those days should be lower than for days with higher PROB-ADO. Thus, if the daily average ADC increases regularly with increasing PROB-ADO levels, it serves as an indicator of the model's validity.

All statistical calculations were performed using the STATGRAPHICS Centurion XVII program (Statgraphics Technologies, Inc.).

2.2. Trend analysis

Finally, a trend analysis assesses the temporal evolution of thermodynamic parameters and PROB-ADO from 1940 to 2021. "openair" data analysis tools (Carslaw and Ropkins, 2012) and the Theil-Sen method (Hirsch et al., 1982) are employed. This statistical procedure, expressing trend magnitude as a positive or negative slope indicating increase or decrease of the magnitude in units per year, is applied to time series of numerical values (Carslaw, 2005; Karanasiou et al., 2014; Querol et al., 2014; Salvador et al., 2015, 2022). Bootstraping techniques determine if trend estimates are statistically significant for a given confidence level. Time series of daily mean values of GT, TPOT, and TANOM and of daily PROB-ADO data, estimated from the multilinear model, provide trend estimates in meters, °C and percentage per year for each study region, respectively. Smoothed trend plots were also generated with "openair". They allow evaluating the time series evolution (Carslaw and Ropkins, 2012).

3. Results and discussion

3.1. Identification of ADO and estimation of daily ADC in the IP and BI domain

The identification procedure (Stage I) results, detailed in supplementary Tables A1-A2, reveal that the proportion of ADO days during 2001–2021 varied across regions. *SE*-IP had the highest percentage at 33 %, while NW-IP and N-IP recorded 9 % and 12 %, respectively. Other regions experienced ADO from 17 % to 25 % of the days. Notably, the highest frequency occurred in summer, ranging from 32 % in NW-IP to 45 % in Central-IP and SE-IP. Spring also exhibited high frequencies, with the lowest in winter (11 % in Central-IP to 18 % in NW-IP).

The average ADC to PM_{10} during ADO days (Stage II) ranged across regions, reaching 15 μg/m^3 in SE-IP and Central-IP, 13 μg/m^3 in SW-IP and NW-IP, and 12 μg/m^3 in NE-IP and BI. N-IP and E-IP recorded 10 to 11 μg/m^3. Average ADC to the annual mean PM_{10} concentration ranged from 1.1 μg/m^3 in NW-IP and N-IP to 4.8 μg/m^3 in SE-IP. These results align with prior studies by Querol et al. (2019b), performed in the same areas for the period 2001–2016, showing a slight increase in event frequency and minimal ADC variation.

The occurrence of ADO days exhibits a distinct negative latitudinal gradient, indicating that the frequency decreases with increasing latitude across the IP-BI domain. However, the intensity of ADO does not exhibit the same latitudinal trend. This implies that intense ADO events can manifest anywhere within the IP-BI domain, irrespective of the frequency with which African air masses reach its sub-regions. This pattern has also been observed over Italy, as documented by Barnaba et al. (2022).

3.2. Selection of assessing parameters

GT, TPOT, and TANOM were chosen as assessing parameters (Stage III) for the reasons exposed in Section 2.1.3.

3.3. Establishing a functional relationship between assessing parameters and ADO

For illustrative purposes, results for the Central-IP zone are discussed. The results for the other regional domains are provided as supplementary material.

It has been observed that the increase in GT, TPOT, and TANOM values from 2001 to 2021 parallels the cumulative number of ADO days. Fig. 4a-c and supplementary Figs. B1-B7 (Stage IV) demonstrate this relationship. Range values, derived from percentile values of the time series, show a consistent increase in the number of ADO days (Fig. 4d-f). This reveals a growing relationship between ADO days and the values of the selected thermodynamic parameters.

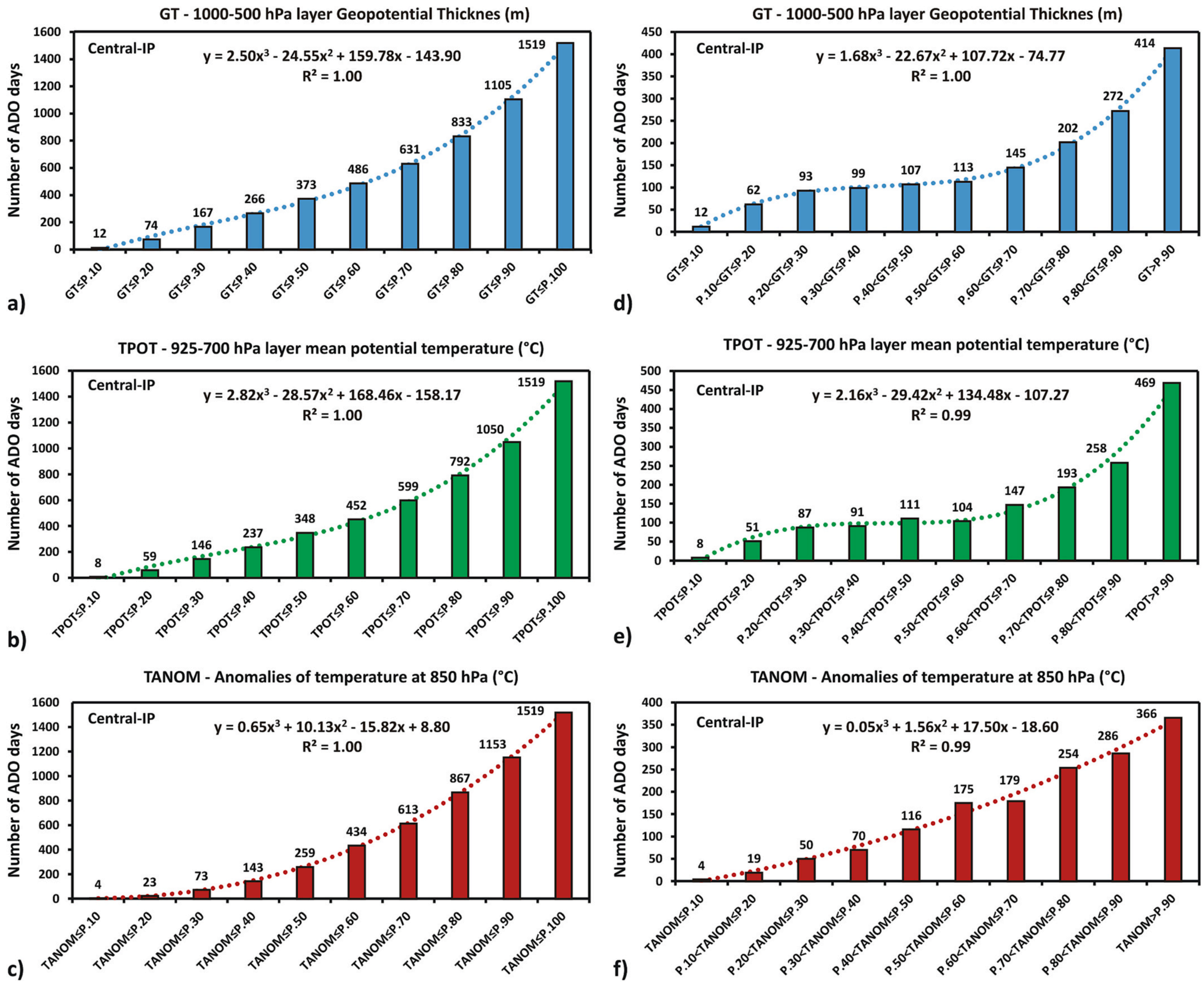

Fig. 4. Number of ADO days for increasing cumulative values of GT (a), TPOT (b) and TANOM (c) (lower than the 10th, 20th,.30th, … and 100th percentile of their time series for the period 2001–2021) and for increasing ranges of values of GT (d), TPOT (e) and TANOM (f) in the central region of the Iberian Peninsula (Central-IP). The ranges of values have been obtained from the percentiles of the time series for the period 2001–2021.

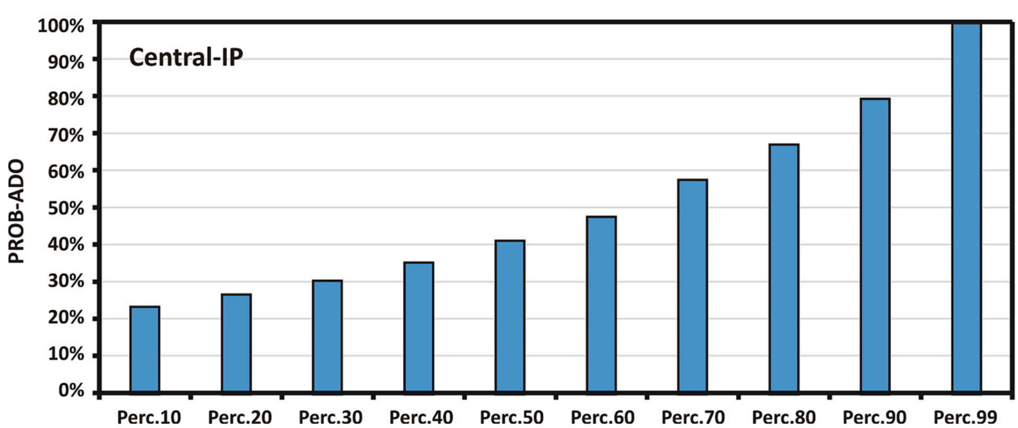

Threshold values of TPOT(°C), TANOM(°C) and GT(m) corresponding to the percentiles of the time series in 2001-2021

	TPOT	TANOM	GT
Perc.10	16.3	-4.1	5418
Perc.20	18.5	-2.6	5467
Perc.30	20.3	-1.4	5500
Perc.40	22.0	-0.4	5531
Perc.50	24.0	0.6	5565
Perc.60	26.3	1.4	5604
Perc.70	29.1	2.4	5647
Perc.80	31.7	3.5	5687
Perc.90	34.2	5.0	5726
Perc.99	38.1	8.3	5779

Fig. 5. Probability of occurrence of African dust outbreaks (PROB-ADO) when exceeding threshold values of GT, TPOT and TANOM (daily mean values) in the central region of the Iberian Peninsula (Central-IP) for all days of the period 2001–2021.

Fig. 4 and supplementary Figs. B1-B7 reveal that the number of ADO days does not linearly increase with the values of the thermodynamic variables but follows a third-degree polynomial function ($R^2 \geq 0.96$ in all cases, Stage IV). This non-linear relationship is explained by a more pronounced increase in ADO above certain variable values, typically between the 70th and 80th percentiles.

3.4. Calculating PROB-ADO when exceeding threshold values of assessing parameters

Threshold values based on percentiles (10th, 20th, …,90th, and 99.9th) of the time series of daily mean values of GT, TPOT, and TANOM were initially chosen (Stage V). For instance, in the Central-IP zone, when 60th percentile values were exceeded (26.3 °C, 1.4 °C, and 5604 m, respectively), 781 ADO episodic days out of the 1633 possible days occurred (Fig. 5). In other words, there is a 47.8 % probability that an ADO event will happen when these threshold values are surpassed (Fig. 5). Consistent with previous findings, as these threshold values increased, the PROB-ADO demonstrated an upward trend (supplementary Table A5).

3.5. Assigning PROB-ADO to all days

The obtained PROB-ADO values once again exhibited a strong fit with those of GT, TPOT, and TANOM through a third-order polynomial function ($R^2 \geq 0.97$ in all cases). This allowed for the determination of threshold values corresponding to any probability value within the range of 0 to 100 % (stage VI of the methodology). Fig. 6 illustrates these functions for the Central-IP zone, along with the threshold values corresponding to PROB-ADO values of 10, 30, 50, 50, 70, and 90 %. Consequently, an estimated PROB-ADO value could be assigned to each day, as elaborated in Section 2.1.6 of the methodology (stage VI). The polynomial functions derived for the other study regions are provided in the supplementary material (Fig. B8).

3.6. Creating a statistical prediction model for daily PROB-ADO

The multi-linear regression procedure, detailed in the methodology section, was applied to the 7670 daily datasets of PROB-ADO, TANOM, TPOT, and GT for the period 2001–2021 across each study region (stage VII of the methodology). Initially, the R^2 parameter's value varied between 77.6 % in the N-IP zone and 83.2 % in the *SE*-IP zone. To enhance the linear fit of the models, the Box-Cox transformation procedure was applied to the dependent variable (Neter et al., 1990). Consequently, the linear fit improved across all regions, resulting in R^2 values ranging from 89.2 % in the BI zone to 91.3 % in the NW-IP zone.

Subsequently, the Durbin-Watson test for autocorrelation was employed to examine the presence of serial correlation in the residuals. This test evaluates the null hypothesis that the residuals are randomly distributed. A rejection of the null hypothesis indicates positive autocorrelation among the error terms, violating one of the essential assumptions for a valid multiple linear regression model. Analysis of the Durbin-Watson statistic revealed autocorrelation in all cases. Therefore, the Cochrane-Orcutt procedure was applied (Neter et al., 1990). Notably, no autocorrelation among residuals or heteroscedasticity in the data was detected in any case. The R^2 values ultimately ranged from 83.7 % in the *SE*-IP zone to 87.5 % in the NW-IP zone (see supplementary Fig. B9). Further details on the Box-Cox and the Cochrane-Orcutt procedures are provided in the supplementary information (Appendix C).

Fig. 7 illustrates the relationship between PROB-ADO values estimated from threshold values and those predicted by the multilinear model in the Central-IP zone. Model equations are also provided.

3.7. Verifying the physical meaning of model estimations

A well-defined seasonal evolution of estimated PROB-ADO values was observed in all regions (Fig. 8, supplementary Tables A6a-A6c). Values in the range 80–100 % occurred mostly between June and August, in the range 50–70 % between May and October, in the range 30–50 % in the transition periods of spring and autumn and in the range 0–30 % between December and March. Thus, the highest values occurred in the warm months, while the lowest were in winter, aligning with the seasonal ADO development in the western Mediterranean basin (Querol et al., 2004, 2019b among others).

Mean daily ADC values increased steadily with rising PROB-ADO in all regions (Fig. 9, supplementary Table A7). Although mean levels were positive from relatively low PROB-ADO ranges (above 20 % in the Central-IP zone), medians were zero until higher PROB-ADO ranges (above 60 % in the Central-IP zone). Lower PROB-ADO ranges mostly contained non-ADO days or days with insignificant ADC. This suggests that for early warning purposes, PROB-ADO values above 60 % are optimal for predicting ADO with significant ADC contributions to regional background levels in the Central-IP region. Positive medians

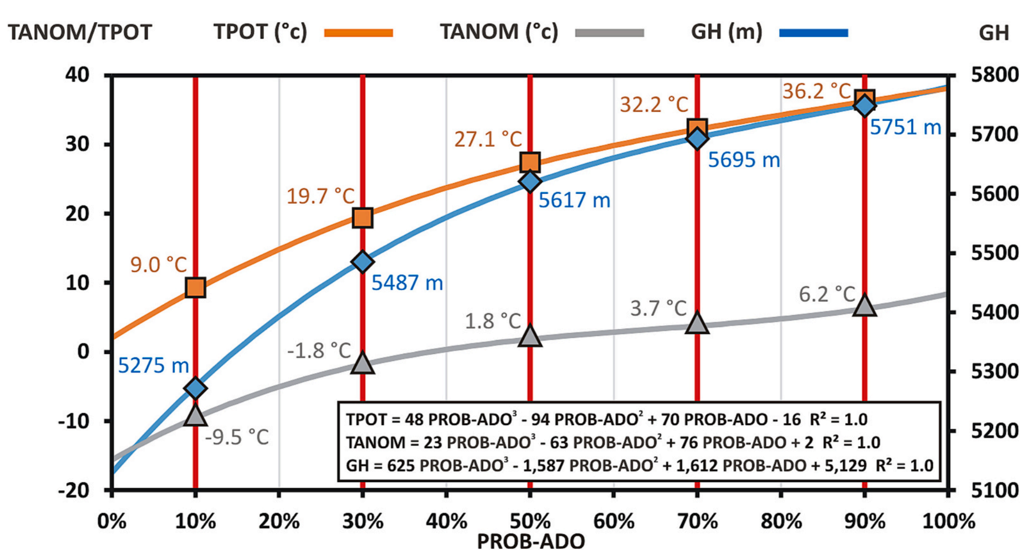

Fig. 6. Polynomial functions representing the threshold values of GT, TPOT and TANOM associated with any probability of occurrence of African dust outbreaks (PROB-ADO) in the central region of the Iberian Peninsula (Central-IP) in 2001–2021. The threshold values for the 10 %, 30 %, 50 %, 70 % and 90 % probabilities have been highlighted.

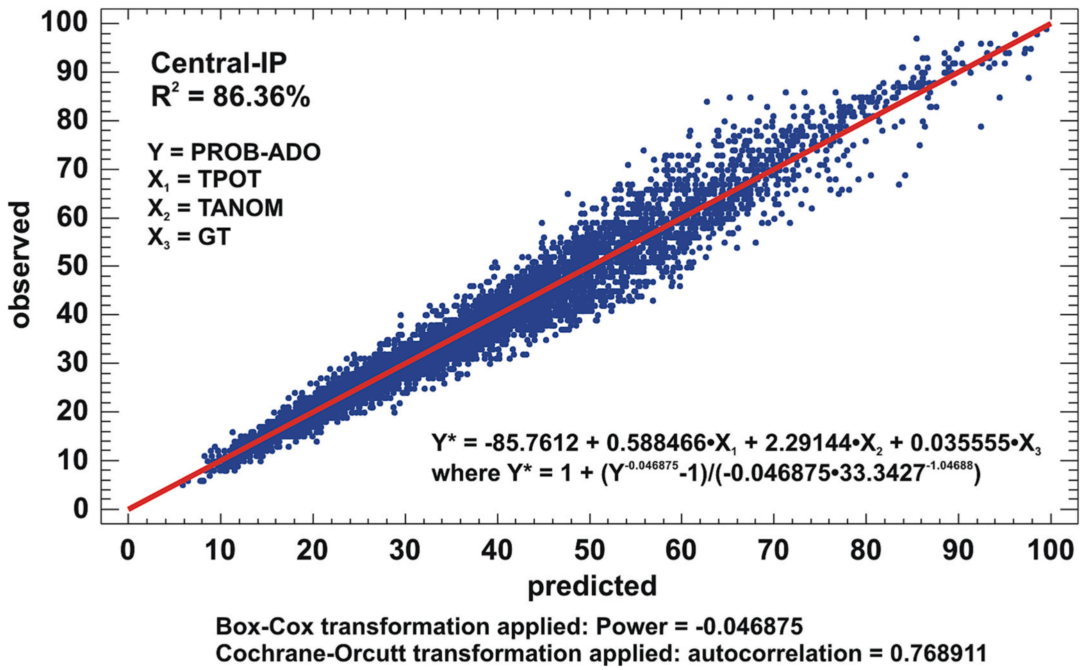

Fig. 7. Comparison of observed probability of occurrence of African dust outbreaks (PROB-ADO) in the central region of the Iberian Peninsula (Central-IP) and predicted with the multilinear regression model in 2001–2021.

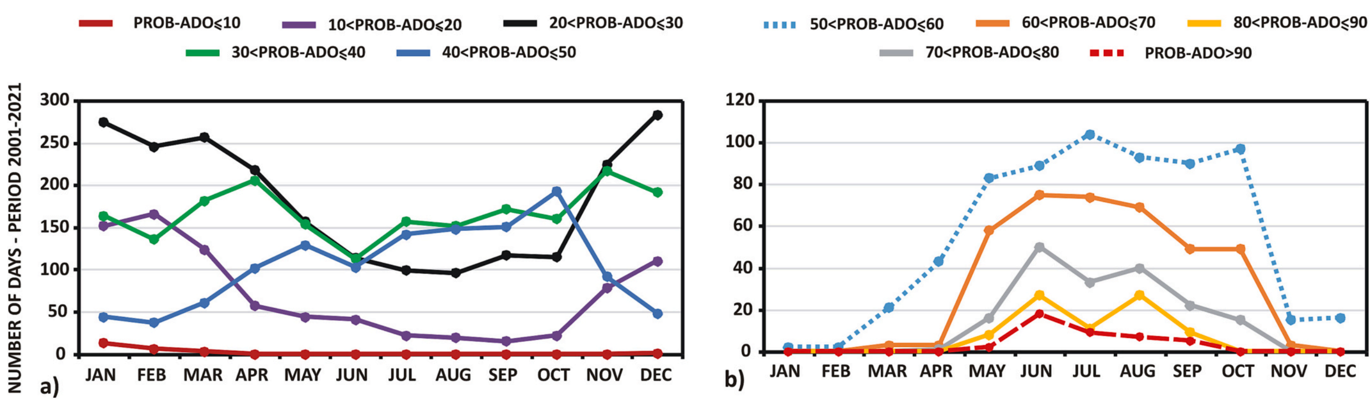

Fig. 8. Total number of days per month with different values of probability of African dust outbreaks occurrence (PROB-ADO) in 2001–2021 in the central region of the Iberian Peninsula (Central-IP).

were observed for PROB-ADO values above 50 % in the NW-IP region, 60 % in the Central-IP, SW-IP, BI, N-IP, and N*E*-IP regions, and 70 % in the SE-IP and E-IP regions (supplementary Table A7). These can be used as threshold warning values for each region, which when forecasted by the models will alert to the potential impact of desert dust on PM levels to which population are exposed.

3.8. Trend analysis

GT, TPOT, and TANOM showed statistically significant increasing trends in all study regions over 1940–2021 (Table 1). Confidence levels ranged from 95 % to 99.9 %, with only the TPOT trend in NW-IP having a confidence level of 90 %. The lowest trends occurred in the NW-IP region (0.229 m/year for GT, 0.011 °C/year for TPOT, and 0.010 °C/year for TANOM), while the highest were in the eastern regions (0.321 m/year for GT in BI, 0.017 °C/year for TPOT in *SE*-IP and NE-IP, and 0.016 °C/year for TANOM in SE-IP, E-IP, and NE-IP). Smoothed trends in the Central-IP area (Fig. 10) revealed more pronounced increases from the mid-1970s for all parameters.

These findings align with the observed surface temperature warming in the Northern Hemisphere throughout the 20th century, characterized by significant temperature increases during the periods 1910–1945 and 1976–2000, primarily attributed to human-induced influences (Marshall, 2001; Gillet et al., 2003; IPCC, 2021).

Given these circumstances, it is unsurprising that a statistically significant positive linear trend, with a confidence level of 99.9 %, was identified for PROB-ADO across all study regions during the 1940–2021 period. The trends varied from 0.018 % per year in the NW-IP region to 0.054 % per year in the SE-IP region (Table 1).

By season (Table 2), PROB-ADO showed statistically significant positive trends at the 99.9 % confidence level in winter for all regions and in summer for all regions except NW-IP. In autumn and spring, positive trends were observed in almost all regions (no trend in NW-IP and N-IP in autumn) but with lower confidence levels (90–95 %) compared to the winter and summer periods.

Regionally, the highest increases in PROB-ADO were observed in E-IP and SE-IP, while the lowest were in N-IP and NW-IP. Increases were higher in summer compared to other seasons (from 0.060 %/year in N-IP to 0.103 %/year in E-IP and SE-IP). Notably, the increase in PROB-ADO was higher in winter (from 0.020 %/year in NW-IP to 0.052 %/year in E-

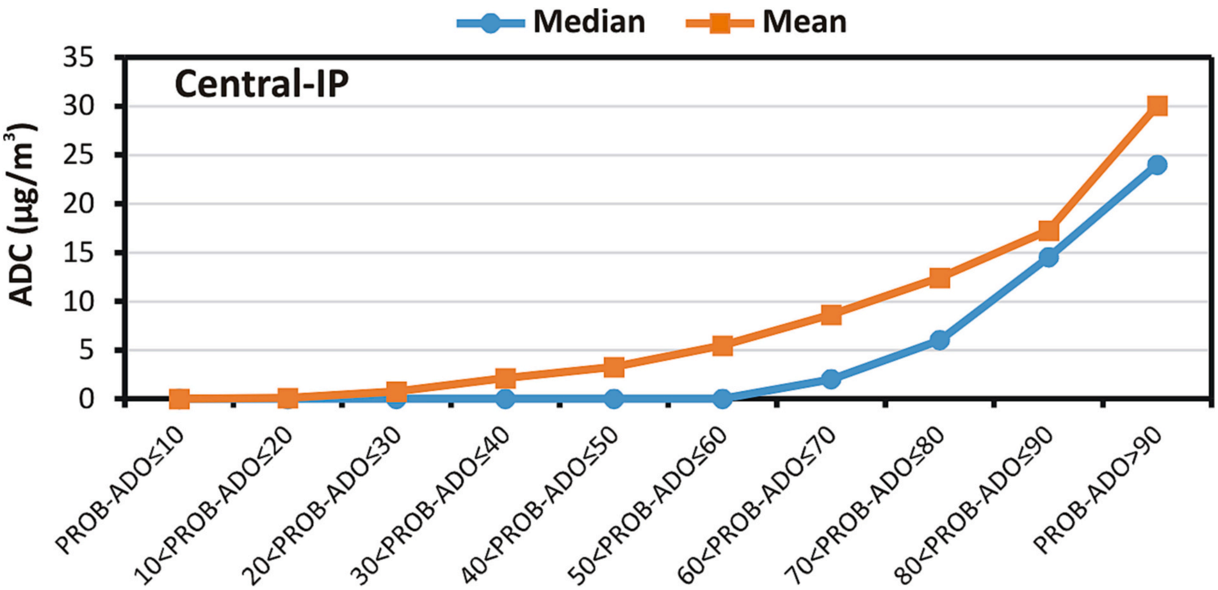

Fig. 9. Mean and median African dust contribution (ADC) values for ranges of probability of occurrence of African dust outbreaks (PROB-ADO) in the central region of the Iberian Peninsula (Central-IP) in 2001–2021.

Table 1
Trend analysis for the mean levels of GT, TPOT and TANOM over each region for the period 1940–2021. Values of the Slope estimator for GT, TPOT and TANOM in m/year, °C/year and °C/year, respectively. IP: Iberian Peninsula; BI: Balearic Islands. ***, * and +: statistically significant value at the 99.9 %, 95 % and 90 % confidence level, respectively.

	SE-IP	SW-IP	Central-IP	E-IP	BI	NW-IP	N-IP	NE-IP
GT	0.319*	0.305*	0.300*	0.312*	0.321*	0.229*	0.273*	0.302*
TPOT	0.017*	0.015*	0.016*	0.017*	0.017*	0.011^{+}	0.014*	0.017*
TANOM	0.016***	0.013***	0.015***	0.016***	0.017***	0.010***	0.014***	0.016***

IP) than in spring (from 0.015 %/year in NW-IP to 0.039 %/year in Central-IP) and autumn (from 0.031 %/year in NE-IP to 0.047 %/year in SE-IP). This aligns with findings of increased winter Saharan dust intrusions over the Western Mediterranean from 2020 to 2022 in comparison with those produced in the period 2003–2019, associated with enhanced blocking activity over the Euro-Atlantic sector (Cuevas-Agulló et al., 2023). Cresswell-Clay et al. (2022) suggest that winters with an extremely large Azores High are more frequent in the industrial era compared to pre-industrial times. The Azores High is a semi-permanent high-pressure system centered near the Azores in the North Atlantic Ocean. This pattern leads to anomalously dry conditions across the western Mediterranean, including the IP. The implications of an increased frequency of an extremely large Azores High include altered atmospheric circulation patterns, potentially influencing weather and climate conditions in the affected regions. The shift towards drier conditions in the western Mediterranean, as mentioned in the context of that study, could have various consequences, including changes in precipitation patterns, water resources, and the occurrence of phenomena like dust outbreaks.

The increasing trends observed in the thermodynamic parameters and PROB-ADO align with the exacerbation of warm conditions in southern Europe over the last decades. This finding supports the hypothesis that ADO are becoming more likely due to global warming. The relationship between climate change and various meteorological and atmospheric phenomena is an area of active research, and studies like this one contribute to our understanding of these complex interactions.

4. Conclusions

This study introduces a methodology for developing models to estimate the daily probability of African dust transport events across various regions in the western Mediterranean basin. Employing thermodynamic variables as assessing parameters and leveraging a catalog of previously identified African dust outbreaks from 2001 to 2021, a functional relationship between assessing parameters and event frequency was established. Through multilinear regression analysis, probability prediction models were generated, demonstrating a strong correlation between the probability of dust events and the variability in daily mean values of these thermodynamic variables.

The study further establishes that days with higher probabilities of occurrence also exhibit elevated dust contributions, indicating a direct relationship between the thermodynamic properties of allochthonous air masses and the transported dust load to the surface. Importantly, each region has a probability threshold value above which the median daily dust contribution surpasses zero, signifying an increased likelihood of impactful African dust events. These threshold values can serve as warning indicators, effectively alerting sensitive populations to the potential occurrence of such events. This methodology aligns with the WHO Air Quality Guidelines requirements, regarding the creation of early warning systems for sand and dust storms to alert the population and take personal measures to minimize their short-term health effects.

The proposed methodology offers a valuable complement to existing numerical forecasting models, which are often complex and resource-intensive. Notably, the simplicity and adaptability of this methodology make it accessible to a broader user base. Since the thermodynamic parameters utilized are typically included in meteorological forecast models, the methodology could be readily applied to calculate daily average values and predict the probability of upcoming African dust events. This information could enhance alert and surveillance systems, serving as a valuable tool for forecasting and complementing surface dust concentration models.

It is crucial to emphasize that the methodology can be employed by

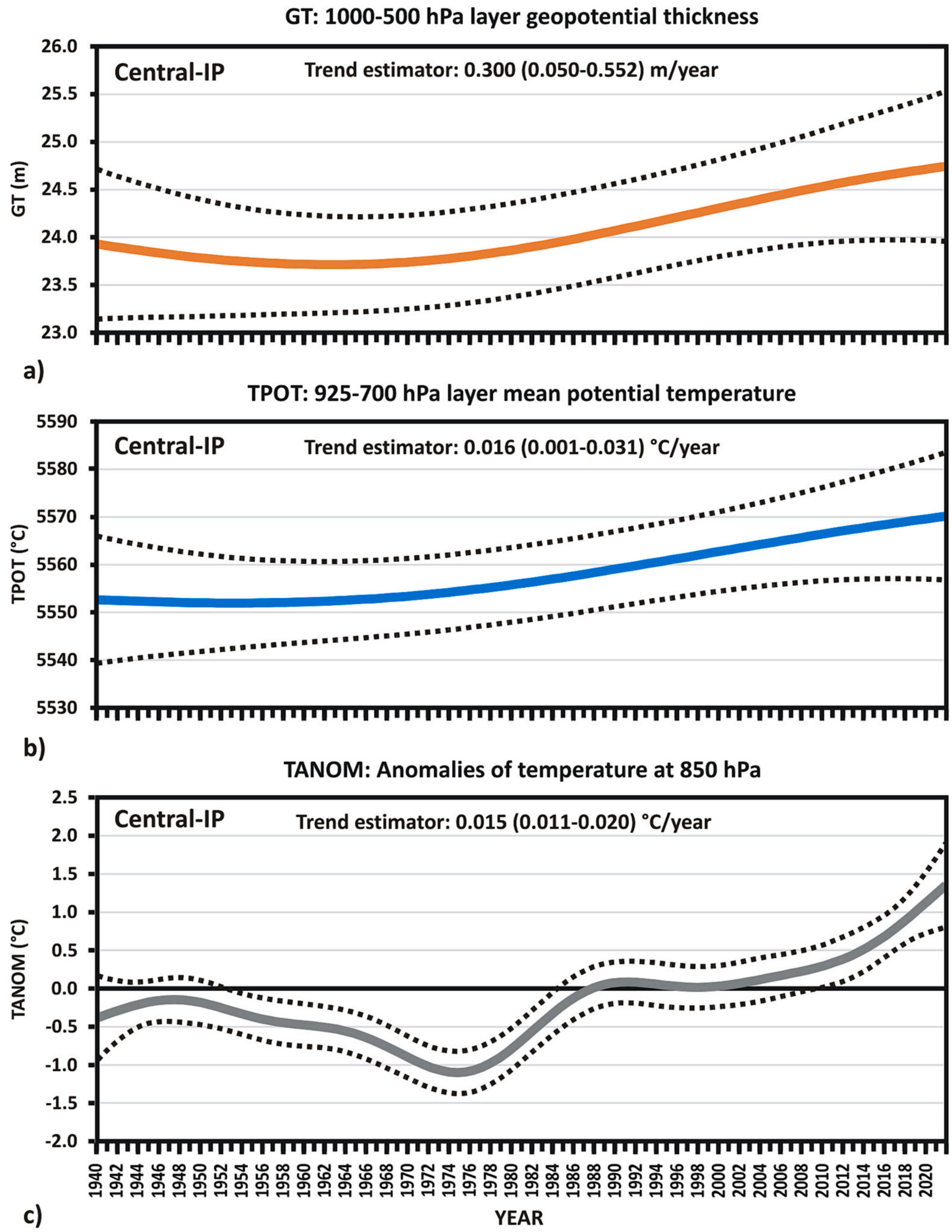

Fig. 10. Smoothed trends (solid line) and 95 % confidence intervals (dashed line) of the monthly mean levels of GT (a), TPOT (b) and TANOM (c) averaged over the central region of the Iberian Peninsula (Central-IP) in the period 1940–2021. Values of the trend estimator and the 95 % confidence interval obtained with the Theil-Sen method are included.

Table 2
Trend analysis for the daily probability of occurrence of African dust outbreaks over each region for the period 1940–2021. Values of the Slope estimator in %/year. IP: Iberian Peninsula; BI: Balearic Islands. ***, * and +: statistically significant value at the 99.9 %, 95 % and 90 % confidence level, respectively, NT: no trend.

	SE-IP	SW-IP	Central-IP	E-IP	BI	NW-IP	N-IP	NE-IP
All period	0.054***	0.046***	0.050***	0.052***	0.043***	0.018***	0.033***	0.040***
Winter	0.050***	0.046***	0.049***	0.052***	0.044***	0.020***	0.035***	0.043***
Spring	0.036+	0.036*	0.039*	0.030+	0.021+	0.015+	0.022+	0.022+
Summer	0.103***	0.069***	0.089***	0.103***	0.084***	NT	0.060***	0.080***
Autumn	0.047*	0.037+	0.039+	0.045*	0.039*	NT	NT	0.031+

various users, adapting to different assessing parameters based on their demonstrated relevance to desert dust outbreak development in a given region.

Global warming can have far-reaching effects on the Earth's climate system, influencing atmospheric circulation patterns, temperature regimes, and the frequency of extreme weather events. In the context of this study, the observed increasing trends in thermodynamic parameters (GT, TPOT, TANOM) across the period 1940–2021 in each of the eight study regions indicate a warming trend in the air masses over the Iberian Peninsula and the Balearic Islands. This warming can contribute to the conditions conducive to the development of African Dust Outbreaks. Examining daily probability results revealed an overall increasing trend in this period. Seasonal trends were also evaluated, showing a consistent rise in the probability of African dust events, even during the less frequent winter period. These trends align with the broader observation that the frequency and intensity of North-African dust outbreaks in the Mediterranean region are likely on the rise due to global warming.

The findings underscore the importance of considering long-term climate trends when studying regional phenomena. The potential implications of more frequent and intense African Dust Outbreaks extend beyond meteorology, impacting air quality, ecosystems, and human health. As global warming continues, understanding these changes becomes crucial for adapting to and mitigating the associated risks.

CRediT authorship contribution statement

Pedro Salvador: Writing – original draft, Visualization, Software, Methodology, Investigation, Formal analysis, Data curation, Conceptualization. **Jorge Pey:** Writing – review & editing, Resources, Project administration, Methodology, Investigation, Funding acquisition, Formal analysis, Conceptualization. **Noemí Pérez:** Writing – review & editing, Visualization, Methodology, Formal analysis, Data curation. **Andrés Alastuey:** Writing – review & editing, Supervision, Resources, Methodology. **Xavier Querol:** Writing – review & editing, Supervision, Resources, Methodology. **Begoña Artíñano:** Writing – review & editing, Supervision, Resources, Methodology.

Declaration of competing interest

The authors declare that they have no known competing financial interests or personal relationships that could have appeared to influence the work reported in this paper.

Data availability

Data will be made available on request.

Acknowledgments

This research received support from the POSAHPI project (Gobierno de España, Agencia Estatal de Investigación, grant PID2019-108101RB-I00), and the ASAH-AS project (Grants for scientific research projects in the National Parks Network for the year 2021, Spanish Ministry for the Ecological Transition and the Demographic Challenge, ref. 2799/2021). The authors extend their gratitude to the NOAA Air Resources Laboratory (ARL) for the provision of the HYSPLIT trajectory model (https://www.arl.noaa.gov/hysplit/hysplit/), the Atmospheric Modelling & Weather Forecasting Group - University of Athens (http://forecast.uoa.gr), the Earth Science Department - Barcelona Supercomputing Centre (https://dust.aemet.es/products/daily-dust-products), the Naval Research Laboratory (https://www.nrlmry.navy.mil/aerosol/) and the NASA (https://worldview.earthdata.nasa.gov/) for the provision of the SKIRON, DREAM/BSC-DREAM8b and MONARCH, NAAPs aerosol maps and the satellite imagery, respectively. Hersbach et al. (2023) was downloaded from the Copernicus Climate Change Service (C3S) (2023). The results contain modified Copernicus Climate Change Service information 2023. Neither the European Commission nor ECMWF is responsible for any use that may be made of the Copernicus information or data it contains.

Appendix A. Supplementary data

Supplementary data to this article can be found online at https://doi.org/10.1016/j.scitotenv.2024.171307.

References

Achilleos, S., Evans, J.S., Yiallouros, P.K., Kleanthous, S., Schwartz, J., Koutrakis, P., 2014. PM10 concentration levels at an urban and background site in Cyprus: the impact of urban sources and dust storms. J. Air Waste Manage. Assoc. 64 (12), 1352–1360.

Ackerman, A.S., Toon, O.B., Stevens, D.E., Heymsfield, A.J., Ramanathan, V., Welton, E.J., 2000. Reduction of tropical cloudiness by soot. Science 288 (5468), 1042–1047. https://doi.org/10.1126/science.288.5468.1042.

Adame, J.A., Notario, A., Cuevas, C.A., Saiz-López, A., 2022. Saharan air outflow variability in the 1980–2020 period. Sci. Total Environ. 839, 156268 https://doi.org/10.1016/j.scitotenv.2022.156268.

Alastuey, A., Querol, X., Wenche, A., Franco, L., Noemí, P., Moreno, T., Cavalli, F., Areskoug, H., Balan, V., Catrambone, M., Ceburnis, D., Cerro, J.C., Conil, S., Gevorgyan, L., Hueglin, C., Imre, K., Jaffrezo, J.L., Leeson, S.R., Mihalopoulos, N., Mitošinková, M., O'Dowd, C.D., Pey, J., Putaud, J.P., Riffault, V., Ripoll, A., Sciare, J., Sellegri, K., Spindler, G., Yttri, K.E., 2016. Geochemistry of PM10 over Europe during the EMEP intensive measurement periods in summer 2012 and winter 2013. Atmos. Chem. Phys. 161 (10), 6107–6129. https://doi.org/10.13039/501100000780.

Aleksandropoulou, V., Lazaridis, M., 2013. Identification of the influence of African dust on PM10 concentrations at the Athens air quality monitoring network during the period 2001–2010. Atmos. Res. 13 (5), 1492–1503.

Alizadeh Choobari, O., Zawar-Reza, P., Sturman, A., 2012. Feedback between windblown dust and planetary boundary-layer characteristics: sensitivity to boundary and surface layer parameterizations. Atmos. Environ. 61, 294–304. https://doi.org/10.1016/j.atmosenv.2012.07.038.

Alizadeh Choobari, O., Zawar-Reza, P., Sturman, A., 2013. Low level jet intensification by mineral dust aerosols. Ann. Geophys. 31 (4), 625–632. https://doi.org/10.5194/angeo-31-625-2013.

Alizadeh Choobari, O., Zawar-Reza, P., Sturman, A., 2014. The global distribution of mineral dust and its impacts on the climate system: a review. Atmos. Res. 138, 152–165. https://doi.org/10.1016/j.atmosres.2013.11.007.

Andreae, M.O., Rosenfeld, D., Artaxo, P., Costa, A.A., Frank, G.P., Longo, K.M., Silva-Dias, M.A.F., 2004. Smoking rain clouds over the Amazon. Science 303 (5662), 1337–1342. https://doi.org/10.1126/science.1092779.

Barnaba, F., Bolignano, A., Di Liberto, L., Morelli, M., Lucarelli, F., Nava, S., Perrino, C., Canepari, S., Basart, S., Costabile, F., Dionisi, D., Ciampichetti, S., Sozzi, R., Gobbi, G.P., 2017. Desert dust contribution to PM10 loads in Italy: methods and recommendations addressing the relevant European Commission Guidelines in support to the Air Quality Directive 2008/50. Atmos. Environ. 161, 288–305. https://doi.org/10.1016/j.atmosenv.2017.04.038.

Barnaba, F., Alvan Romero, N., Bolignano, A., Basart, S., Renzi, M., Stafoggia, M., 2022. Multiannual assessment of the desert dust impact on air quality in Italy combining PM10 data with physics-based and geostatistical models. Environ. Int. 163, 107204 https://doi.org/10.1016/j.envint.2022.107204.

Basart, S., Perez, C., Cuevas, E., Baldasano, J.M., Gobbi, G.P., 2009. Aerosol characterization in Northern Africa, Northeastern Atlantic, Mediterranean Basin and Middle East from direct-sun AERONET observations. Atmos. Chem. Phys. 9, 8265–8282. https://doi.org/10.5194/acp-9-8265-2009.

Carslaw, D.C., 2005. Evidence of an increasing NO2/NOx emissions ratio from road traffic emissions. Atmos. Environ. 39, 4793–4802.

Carslaw, D.C., Ropkins, K., 2012. Openair - an R package for air quality data analysis. Environ. Model Softw. 27-28, 52–61.

Christensen, J.H., 1997. The Danish eulerian hemispheric model - a three-dimensional air pollution model used for the Arctic. Atmos. Environ. 31, 4169–4191.

Commission Staff Working Paper, Establishing guidelines for demonstration and subtraction of exceedances attributable to natural sources under the Directive 2008/50/EC on ambient air quality and cleaner air for Europe, Brussels, 15.02.2011. SEC (2011) 208 final. Available online at: https://www.miteco.gob.es/content/dam/miteco/es/calidad-y-evaluacion-ambiental/temas/atmosfera-y-calidad-del-aire/Directrices%20Comisi%C3%B3n-SEC%20208%20final-en_tcm30-186523.pdf (Last access: February 2024).

Cook, B.I., Miller, R.L., Seager, R., 2009. Amplification of the North American "dust bowl" drought through human induced land degradation. Proc. Natl. Acad. Sci. USA 106, 4997–5001.

Copernicus Climate Change Service (C3S) (2023): ERA5 hourly data on pressure levels from 1940 to present. Copernicus Climate Change Service (C3S) Climate Data Store (CDS). 10.24381/ cds.bd0915c6 (Accessed on 23-JUN-2023).

Cresswell-Clay, N., Ummenhofer, C.C., Thatcher, D.L., Wanamaker, A.D., Denniston, R.F., Asmerom, Y., Polyak, V.J., 2022. Twentieth-century Azores High expansion unprecedented in the past 1,200 years. Nat. Geosci. 15, 548–553. https://doi.org/10.1038/s41561-022-00971-w.

Cuevas-Agulló, E., Barriopedro, D., García, R.D., Alonso-Pérez, S., González-Alemán, J.J., Werner, E., Suárez, D., Bustos, J.J., García-Castrillo, G., García, O., Barreto, Á., Basart, S., 2023. Sharp increase of Saharan dust intrusions over the Western Mediterranean and Euro-Atlantic region in winters 2020–2022 and associated atmospheric circulation. EGUsphere [preprint]. https://doi.org/10.5194/egusphere-2023-1749.

Díaz, J., Linares, C., Carmona, R., Russo, A., Ortiz, C., Salvador, P., Machado Trigo, R., 2017. Saharan dust intrusions in Spain: health impacts and associated synoptic conditions. Environ. Res. 156, 455–467.
Escudero, M., Querol, X., Ávila, A., Cuevas, E., 2007a. Origin of the exceedances of the European daily PM limit value in regional background areas of Spain. Atmos. Environ. 41, 730–744.
Escudero, M., Querol, X., Pey, J., Alastuey, A., Pérez, N., Ferreira, F., Cuevas, E., Rodríguez, S., Alonso, S., 2007b. A methodology for the quantification of the net African dust load in air quality monitoring networks. Atmos. Environ. 41, 5516–5524.
Galvin, J.F.P, 2016. An introduction to the meteorology and climate of the tropics. Wiley-Blackwell, ISBN 978-1-119-08623-9, p. 336.
Gill, T.E., 1996. Eolian sediments generated by anthropogenic disturbance of playas: human impacts on the geomorphic system and geomorphic impacts on the human system. Geomorphology 17, 207–228.
Gillet, N. P., Graf, H. F., Osborn, T. J., 2003. Climate Change and the North Atlantic Oscillation. Chapter in The North Atlantic Oscillation: Climatic Significance and Environmental Impact. Published by the American Geophysical Union as part of the Geophysical Monograph Series, 134. Washington, DC, Editor(s): Hurrell, J.W., Kushnir, Y., Ottersen, G. & Visbeck, M., https://doi.org/10.1029/134GM09.
Ginoux, P., Garbuzov, D., Hsu, H.C., 2010. Identification of anthropogenic and natural dust sources using Moderate Resolution Imaging Spectroradiometer (MODIS) deep blue level 2 data. J. Geophys. Res. 115, D05204 https://doi.org/10.1029/2009JD012398.
Ginoux, P., Prospero, J.M., Gill, T.E., Hsu, N.C., Zhao, M., 2012. Global-scale attribution of anthropogenic and natural dust sources and their emission rates based on MODIS deep blue aerosol products. Rev. Geophys. 50, RG3005 https://doi.org/10.1029/2012RG000388.
Goudie, A.S., 2014. Desert dust and human health disorders. Environ. Int. 63, 101–113.
Goudie, A.S., Middleton, N.J., 2001. Saharan dust storms: nature and consequences. Earth Sci. Rev. 56, 179–204.
Griffin, D.W., 2007. Atmospheric movement of microorganisms in clouds of desert dust and implications for human health. Clin. Microbiol. Rev. 20, 459–477.
Heffernan, O., 2016. The mystery of the expanding tropics. Nature 530, 20–22.
Hersbach, H., Bell, B., Berrisford, P., Biavati, G., Horányi, A., Muñoz Sabater, J., Nicolas, J., Peubey, C., Radu, R., Rozum, I., Schepers, D., Simmons, A., Soci, C., Dee, D., Thépaut, J-N., 2023. ERA5 hourly data on pressure levels from 1940 to present. Copernicus Climate Change Service (C3S) Climate Data Store (CDS), DOI: 10.24381/cds.bd0915c6 (Accessed on 23-JUN-2023).
Hirsch, R., Slack, J.R., Smith, R.A., 1982. Techniques of trend analysis for monthly water quality data. Water Resour. Res. 18, 107–121.
Hooper, J., Marx, S., 2018. A global doubling of dust emissions during the Anthropocene? Glob. Planet. Chang. 169, 70–91. https://doi.org/10.1016/j.gloplacha.2018.07.003.
Huneeus, N., Schulz, M., Balkanski, Y., Griesfeller, J., Prospero, J., Kinne, S., Bauer, S., Boucher, O., Chin, M., Dentener, F., Diehl, T., Easter, R., Fillmore, D., Ghan, S., Ginoux, P., Grini, A., Horowitz, L., Koch, D., Krol, M.C., Landing, W., Liu, X., Mahowald, N., Miller, R., Morcrette, J.-J., Myhre, G., Penner, J., Perlwitz, J., Stier, P., Takemura, T., Zender, C.S., 2011. Global dust model intercomparison in AeroCom phase I. Atmos. Chem. Phys. 11, 7781–7816.
IPCC, 2021. Climate Change 2021: The Physical Science Basis. Contribution of Working Group I to the Sixth Assessment Report of the Intergovernmental Panel on Climate Change. Masson-Delmotte, V., P. Zhai, A. Pirani, S.L. Connors, C. Péan, S. Berger, N. Caud, Y. Chen, L. Goldfarb, M.I. Gomis, M. Huang, K. Leitzell, E. Lonnoy, J.B.R. Matthews, T.K. Maycock, T. Waterfield, O. Yelekçi, R. Yu, and B. Zhou (eds.). Cambridge University Press, Cambridge, United Kingdom and New York, NY, USA, In press, doi:https://doi.org/10.1017/9781009157896.
IPCC, 2023. Climate Change 2022 – Impacts, Adaptation and Vulnerability: Working Group II Contribution to the Sixth Assessment Report of the Intergovernmental Panel on Climate Change. Cambridge University Press, Cambridge. https://doi.org/10.1017/9781009325844.
Justice, C.O., Townshend, J.R.G., Vermote, E.F., Masuoka, E., Wolfe, R.E., Saleous, N., Roy, D.P., Morisette, J.T., 2002. An overview of MODIS land data processing and product status. Remote Sens. Environ. 83, 3–15. https://doi.org/10.1016/S0034-4257(02)00084-6.
Kallos, G., Papadopoulos, A., Katsafados, P., Nickovic, S., 2006. Transatlantic Saharan dust transport: model simulation and results. J. Geophys. Res. 111, D09204 https://doi.org/10.1029/2005JD006207.
Karanasiou, A., Querol, X., Alastuey, A., Perez, N., Pey, J., Perrino, C., Berti, G., Gandini, M., Poluzzi, V., Ferrari, S., de la Rosa, J., Pascal, M., Samoli, E., Kelessis, A., Sunyer, J., Alessandrini, E., Stafoggia, M., Forastiere, F., the MED-PARTICLES Study Group, 2014. Particulate matter and gaseous pollutants in the Mediterranean Basin: results from the MED-PARTICLES project. Sci. Total Environ. 488-489, 297–315.
Kok, J.F., Ridley, D.A., Zhou, Q., Miller, R.L., Zhao, C., Heald, C.L., Ward, D.S., Albani, S., Haustein, K., 2017. Smaller desert dust cooling effect estimated from analysis of dust size and abundance. Nat. Geosci. 10 (4), 274–278.
Koren, I., Kaufman, Y.J., Remer, L.A., Kaufman, Y.J., Remer, L.A., Koren, I., Martins, J. V., Martins, J.V., 2004. Measurement of the effect of Amazon smoke on inhibition of cloud formation. Science 303 (5662), 1342–1345. https://doi.org/10.1126/science.1089424.
Kubilay, N., Nickovic, S., Moulin, C., Dulac, F., 2000. An illustration of the transport of mineral dust onto the eastern Mediterranean. Atmos. Environ. 34, 1293–1303.
Lee, J.A., Baddock, M.C., Mbuh, M.J., Gill, T.E., 2012. Geomorphic and land cover characteristics of aeolian dust sources in West Texas and eastern New Mexico, USA. Aeolian Res. 3 (4), 459–466.
Ma, R., Duan, H., Hu, C., Feng, X., Li, A., Ju, W., Jiang, J., Yang, G., 2010. A half-century of changes in China's lakes: global warming or human influence? Geophys. Res. Lett. 37, L24106 https://doi.org/10.1029/2010GL045514.
Marshall, J., 2001. North Atlantic climate variability: phenomena, impacts and mechanisms. Int. J. Climatol. 21 (15), 1863–1898.
Miller, R.L., Tegen, I., 1998. Climate response to soil dust aerosols. J. Clim. 11 (12), 3247–3267.
Moulin, C., Lambert, C.E., Dayan, U., Masson, V., Ramonet, M., Bousquet, P., Legrand, M., Balkanski, Y.J., Guelle, W., Marticorena, B., Bergametti, G., Dulac, F., 1998. Satellite climatology of African dust transport in the Mediterranean atmosphere. J. Geophys. Res. 103 (D11), 13137–13144.
Neff, J.C., Ballantyne, A.P., Farmer, G.L., Mahowald, N.M., Conroy, J.L., Landry, C.C., Overpeck, J.T., Painter, T.H., Lawrence, C.R., Reynolds, R.L., 2008. Increasing eolian dust deposition in the western United States linked to human activity. Nat. Geosci. 1, 189–195.
Neter, J., Wasserman, W., Kutner, M.H., 1990. Applied Linear Statistical Models: Regression, Analysis of Variance, and Experimental Designs, Third edition. Richard D. Irwin, Inc. ISBN 0-256-08338-X. 1181 pp.
Orlove, B., 2005. Human adaptation to climate change: a review of three historical cases and some general perspectives. Environ. Sci. Pol. 8, 589–600.
Orlovsky, N., Orlovsky, L., Durdyev, A., 2005. Dust storms in Turkmenistan. J. Arid Environ. 60 (1), 83–97.
Pandolfi, M., Tobias, A., Alastuey, A., Sunyer, J., Schwartz, J., Lorente, J., Pey, J., Querol, X., 2014. Effect of atmospheric mixing layer depth variations on urban air quality and daily mortality during Saharan dust outbreaks. Sci. Total Environ. 494, 283–289.
Pérez, L., Tobias, A., Querol, X., Künzli, N., Pey, J., Alastuey, A., Viana, M., Valero, N., González-Cabré, M., Sunyer, J., 2008. Coarse particles from Saharan dust and daily mortality. Epidemiology 19 (6), 800–807.
Pérez, C., Haustein, K., Janjic, Z., Jorba, O., Huneeus, N., Baldasano, J.M., Black, T., Basart, S., Nickovic, S., Miller, R.L., Perlwitz, J.P., Schulz, M., Thomson, M., 2011. Atmospheric dust modeling from meso to global scales with the online NMMB/BSC-dust model – part 1: model description, annual simulations and evaluation. Atmos. Chem. Phys. 11, 13001–13027. https://doi.org/10.5194/acp-11-13001-2011.
Pérez, L., Tobías, A., Pey, J., Pérez, N., Alastuey, A., Sunyer, J., Querol, X., 2012. Effects of local and Saharan particles on cardiovascular disease mortality. Epidemiology 23, 768–769.
Pey, J., Querol, X., Alastuey, A., Forastiere, F., Stafoggia, M., 2013. African dust outbreaks over the Mediterranean Basin during 2001-2011: PM10 concentrations, phenomenology and trends, and its relation with synoptic and mesoscale meteorology. Atmos. Chem. Phys. 13, 1395–1410.
Prospero, J.M., Lamb, P.J., 2003. African droughts and dust transport to the Caribbean: climate change implications. Science 302 (5647), 1024–1027. https://doi.org/10.1126/science.1089915.
Prospero, J.M., Ginoux, P., Torres, O., Nicholson, S.E., Gill, T.E., 2002. Environmental characterization of global sources of atmospheric soil dust identified with the Nimbus 7 Total Ozone Mapping Spectrometer (TOMS) absorbing aerosol product. Rev. Geophys. 40 (1), 1002. https://doi.org/10.1029/2000RG000095.
Querol, X., Alastuey, A., Puicercus, J.A., Mantilla, E., Miró, J.V., López-Soler, A., Plana, F., Artíñano, B., 1998. Seasonal evolution of suspended particles around a large coal-fired power station: particles levels and sources. Atmos. Environ. 32, 1963–1978.
Querol, X., Alastuey, A., Rodriguez, S., Viana, M., Artíñano, B., Salvador, P., Mantilla, E., Garcia, S., Fernandez, R., de la Rosa, J., Sanchez, A., Menendez, M., 2004. Levels of PM in rural, urban and industrial sites in Spain. Sci. Total Environ. 334–335, 359–376.
Querol, X., Alastuey, A., Pey, J., Pandolfi, M., Cusack, M., Pérez, N., Viana, M., Moreno, T., Mihalopoulos, N., Kallos, G., Kleanthous, S., 2009. African dust contributions to mean ambient PM10 mass-levels across the Mediterranean Basin. Atmos. Environ. 43 (28), 4266–4277.
Querol, X. et al., 2013. Procedimiento Para Identificación de Episodios Naturales Africanos de PM_{10} y $PM_{2.5}$, y la Demostración de Causa en lo Referente a las Superaciones del Valor Límite Diario de PM_{10}. (Scientific Report published by the Spanish Ministry of Agriculture, Food and Environment and the Portuguese Environmental Agency, Madrid, Spain). Available online at: https://www.miteco.gob.es/content/dam/miteco/es/calidad-y-evaluacion-ambiental/temas/atmosfera-y-calidad-del-aire/metodologiaparaepisodiosnaturales-revabril2013_tcm30-186522.pdf (Last access February 2024).
Querol, X., Alastuey, A., Pandolfi, M., Reche, C., Perez, N., Minguillón, M.C., Moreno, T., Viana, M., Escudero, M., Orio, A., Pallares, M., Reina, F., 2014. 2001-2012 trends on air quality in Spain. Sci. Total Environ. 490, 957–969.
Querol, X., Tobías, A., Pérez, N., Karanasiou, A., Amato, F., Stafoggia, M., Pérez García-Pando, C., Ginoux, P., Forastiere, F., Gumy, S., Mudu, P., Alastuey, A., 2019a. Monitoring the impact of desert dust outbreaks for air quality studies. Environ. Int. 130, 104867 https://doi.org/10.1016/j.envint.2019.05.061.
Querol, X., Pérez, N., Reche, C., Ealo, M., Ripoll, A., Tur, J., Pandolfi, M., Pey, J., Salvador, P., Moreno, T., Alastuey, A., 2019b. African dust and air quality over Spain: is it only dust that matters? Sci. Total Environ. 686, 737–752. https://doi.org/10.1016/j.scitotenv.2019.05.349.
Rodríguez, S., Querol, X., Alastuey, A., Kallos, G., Kakaliagou, O., 2001. Saharan dust contributions to PM10 and TSP levels in southern and eastern Spain. Atmos. Environ. 35, 2433–2447.
Rosenfeld, D., Woodley, W.L., 2000. Deep convective clouds with sustained supercooled liquid water down to −37.5 degrees C. Nature 405 (6785), 440–442.
Salvador, P., Artíñano, B., Molero, F., Viana, M., Pey, J., Alastuey, A., Querol, X., 2013. African dust contribution to ambient aerosol levels across central Spain:

characterization of long-range transport episodes of desert dust. Atmos. Res. 127, 117–129.

Salvador, P., Alonso, S., Pey, J., Artíñano, B., de Bustos, J.J., Alastuey, A., Querol, X., 2014. African dust outbreaks over the western Mediterranean basin: 11 year characterization of atmospheric circulation patterns and dust source areas. Atmos. Chem. Phys. 14, 6759–6775. https://doi.org/10.5194/acp-14-6759-2014.

Salvador, P., Artíñano, B., Viana, M.M., Alastuey, A., Querol, X., 2015. Multicriteria approach to interpret the variability of the levels of particulate matter and gaseous pollutants in the Madrid metropolitan area, during the 1999-2012 period. Atmos. Environ. 109, 205–216.

Salvador, P., Molero, F., Fernández, A.J., Tobías, A., Pandolfi, M., Gómez-Moreno, F.J., Barreiro, M., Pérez, N., Martínez Marco, I., Revuelta, M.A., Querol, X., Artíñano, B., 2019. Synergistic effect of the occurrence of African dust outbreaks on atmospheric pollutant levels in the Madrid metropolitan area. Atmos. Res. 226, 208–218.

Salvador, P., Pey, J., Pérez, N., Querol, X., Artíñano, B., 2022. Increasing atmospheric dust transport towards the western Mediterranean over 1948–2020. NPJ Clim. Atmos. Sci. 5, 34. https://doi.org/10.1038/s41612-022-00256-4.

Sánchez-Benítez, A., García-Herrera, R., Barriopedro, D., Sousa, P.M., Trigo, R.M., 2018. June 2017: the earliest European summer mega-heatwave of reanalysis period. Geophys. Res. Lett. 45, 1955–1962. https://doi.org/10.1002/2018GL077253.

Sokolik, I., Toon, O., 1996. Direct radiative forcing by anthropogenic airborne mineral aerosols. Nature 381 (6584), 681–683.

Sousa, P.M., Barriopedro, D., Ramos, A.M., García-Herrera, R., Espírito-Santo, F., Trigo, R.M., 2019. Saharan air intrusions as a relevant mechanism for Iberian heatwaves: the record breaking events of August 2018 and June 2019. Weather. Clim. Extremes 26, 100224. https://doi.org/10.1016/j.wace.2019.100224.

Stafoggia, M., the MED-PARTICLES Study Group, 2016. Desert dust outbreaks in southern Europe: contribution to daily PM10 concentrations and short-term associations with mortality and hospital admissions. Environ. Health Perspect. 124, 413–419.

Stein, A.F., Draxler, R.R., Rolph, G.D., Stunder, B.J.B., Cohen, M.D., Ngan, F., 2015. NOAA's HYSPLIT atmospheric transport and dispersion modeling system. Bull. Am. Meteorol. Soc. 96, 2059–2077. https://doi.org/10.1175/BAMS-D-14-00110.1.

Stout, J.E., 2001. Dust and environment in the southern High Plains of North America. J. Arid Environ. 47, 425–441.

Su, J., Huang, J., Fu, Q., Minnis, P., Ge, J., Bi, J., 2008. Estimation of Asian dust aerosol effect on cloud radiation forcing using Fu-Liou radiative model and CERES measurements. Atmos. Chem. Phys. 8 (10), 2763–2771. https://doi.org/10.5194/acp-8-2763-2008.

Tegen, I., Lacis, A., Fung, I., 1996. The influence on climate forcing of mineral aerosols from disturbed soils. Nature 380 (6573), 419–422.

Tegen, I., Werner, M., Harrison, S.P., Kohfeld, K.E., 2004. Relative importance of climate and land use in determining present and future global soil dust emission. Geophys. Res. Lett. 31, L05105 https://doi.org/10.1029/2003GL019216.

Textor, C., Schulz, M., Guibert, S., Kinne, S., Balkanski, Y., Bauer, S., Berntsen, T., Berglen, T., Boucher, O., Chin, M., Dentener, F., Diehl, T., Easter, R., Feichter, H., Fillmore, D., Ghan, S., Ginoux, P., Gong, S., Grini, A., Hendricks, J., Horowitz, L., Huang, P., Isaksen, I., Iversen, I., Kloster, S., Koch, D., Kirkevåg, A., Kristjansson, J. E., Krol, M., Lauer, A., Lamarque, J.F., Liu, X., Montanaro, V., Myhre, G., Penner, J., Pitar, G., Reddy, S., Seland, Ø., Stier, P., Takemura, T., Tie, X., 2006. Analysis and quantification of the diversities of aerosol life cycles within AeroCom. Atmos. Chem. Phys. 6, 1777–181.

Thomas, N., Nigam, S., 2018. Twentieth-century climate change over Africa: seasonal hydroclimate trends and Sahara Desert expansion. J. Clim. 31, 3349–3370. https://doi.org/10.1175/JCLI-D-17-0187.1.

Tobias, A., Karanasiou, A., Amato, F., Roqué, M., Querol, X., 2019a. Health effects of desert dust and sand storms: a systematic review and meta-analysis protocol. BMJ Open 2019 (9), e029876. https://doi.org/10.1136/bmjopen-2019-029876.

Tobias, A., Karanasiou, A., Amato, F., Querol, X., 2019b. Health effects of desert dust and sand storms: a systematic review and meta-analysis. Environmental Epidemiology. 3, 396. https://doi.org/10.1097/01.EE9.0000610424.75648.58.

Varga, G., 2012. Spatio-temporal distribution of dust storms—a global coverage using NASA TOMS aerosol measurements. Hung. Geogr. Bull. 61, 275–298.

Viana, M., Salvador, P., Artíñano, B., Querol, X., Alastuey, A., Pey, J., Latz, A.J., Cabañas, M., Moreno, T., García, S., Herce, M., Diez, P., Romero, D., Fernández, R., 2010. Assessing the performance of methods to detect and quantify African dust in airborne particulates. Environ. Sci. Technol. 44, 8814–8820.

Wallace, J.M., Hobbs, P.V., 2006. Atmospheric Science – An Introductory Survey, second ed. Elsevier, Canada.

Washington, R., Todd, M., Middleton, N., Goudie, A.S., 2003. Global dust storm source areas determined by the Total Ozone Monitoring Spectrometer and ground observations. Ann. Assoc. Am. Geogr. 93, 297–313.

WHO Global Air Quality Guidelines. Particulate Matter (PM2.5 and PM10), Ozone, Nitrogen Dioxide, Sulfur Dioxide and Carbon Monoxide, 2021. World Health Organization, Geneva (Licence: CC BY-NC-SA 3.0 IGO).

Yu, H., Chin, M., Yuan, T., Bian, H., Remer, L.A., Prospero, J.M., Omar, A., Winker, D., Yang, Y., Zhang, Y., Zhang, Z., Zhao, C., 2015. The fertilizing role of African dust in the Amazon rainforest: a first multiyear assessment based on data from Cloud-Aerosol Lidar and Infrared Pathfinder Satellite Observations. Geophys. Res. Lett. 42, 1984–1991. https://doi.org/10.1002/2015GL063040.

Zucca, C., Middelton, N., Kang, U., Liniger, H., 2021. Shrinking water bodies as hotspots of sand and dust storms: the role of land degradation and sustainable soil and water management. Catena 207, 105669.